Chapter-6

(Mechano-chemically synthesized high alumina cements and their implementation as low cement castables with some micro-fine additives)

Mechano-chemically synthesized high alumina cements and their implementation as low cement castables with some micro-fine additives

6.1 Introduction

High-energy ball milling process, known as mechanochemical method for simultaneous excessive grinding with occurrence of chemical reactions, is being utilized for mechanically activation of ceramic powders to obtain nano size particle size distributions. These finely ground powders show low temperature solid state reactions (Wang et al., 2008; Jung et al., 2010). The process can also be helpful in selecting low-cost commercially available oxides and can produce powders of nanometer size (Fahami et al., 2014). On the other hand, high alumina cement provides high service temperature when used as refractory castables. Therefore, the effects of high-energy ball milling and subsequent calcinations on the formation of high alumina cementing phases, using mixtures of Al_2O_3 and $CaCO_3$, were investigated.

Recently, mechanochemical reaction has emerged as a beneficial and low cost method to produce nano scale materials (Ye and Troczynski, 2007). This technique generally influences texture and structure of final sintered products (Hawari and Johan, 2011). Mechanical activation can also be employed in order to improve the kinetics of adsorption, catalysis and mineral synthesis as well as to customize the mineral surfaces with respect to structure and composition. Modifying the structure, composition and reactivity of the mineral surface gives rise to new applications and products (Kleiv and Thornhill, 2006). It has been reported by many researchers that the mechanochemical processing can be designed to synthesize nano-crystalline particles dispersed within a soluble salt matrix. The chemical precursors react, either during milling or in the subsequent heat treatment stage (Guha, 1997, Citak, 1999).

Nano sized high alumina cements (HACs) powders were synthesized by mechanochemical treatment of Al_2O_3 and $CaCO_3$ mixtures in weight ratio of 7:3 and 8:2. This chapter also compares the calcined high alumina cements obtained by mechanically activated precursor mixes for milling 1h, 2h and 3h, respectively. The reactions between Al_2O_3 and $CaCO_3$ towards cementing phase formation were obtained at much lower temperatures (~1000°C). The reactions of the oxides are initiated at temperatures as low as 900°C. Two compositions of calcium aluminate powders containing 70 and 80 wt% Al_2O_3 were selected. The prepared cements were characterized for their structural, mechanical and cementing properties. Finally, the calcination temperature and time were optimized to obtain desired phases in the HAC. The effect of high-energy ball milling on the fineness of the mixtures, microstructure development of the milled powders, cementing properties and phase formation were investigated. The prime cementing phases observed were CA, CA_2 and CA_6.

Low cement castables were prepared using calcined Chinese bauxite as aggregate matrix, prepared HACs powders as hydraulic binder and micro-fine additives as pore filling agents. The bonding properties of high alumina cements as well as sinterability in these castables were studied with inclusions of ZrO2, α-Al_2O_3 and SiC as micro-fine additives. α-alumina is most stable and technically useful crystalline form. It has a crystal structure based on hexagonal close packing of oxygen ions with aluminum ions occupying two out of every eight octahedral voids. Inter atomic bonding, though generally taken to be ionic, has significant covalent component (Studart et al., 2001). As a result, commercial alumina is difficult to sinter and requires high temperature around 1700˚C for any significant densification. It is therefore necessary to obtain alumina in a reactive form with submicron particle size to carryout sintering at temperature below 1550˚C. Zirconia is considered as high temperature sustaining engineering material because it shows good chemical stability, high compressive strength and good fracture strength even at high temperatures along with low thermal expansion coefficient. This complex refractory formulation was chosen, keeping in mind the severe operating conditions of

secondary steelmaking and ever demanding clean steel process requirements. Alumina-zirconia based monoliths are being used in sliding gate plates, submerged entry nozzles and ladle shrouds. Due to continuous casting operations these complex refractory shapes suffer degradation due to high abrasion. Only alumina-zirconia based materials are found to survive in such operations. Carbon is sometimes added to prevent wettability from molten metal but it has very low oxidation resistance. So, sub-micron sized silicon carbide was used in the present work to develop similar performance. Silicon carbide is very hard material. Its addition may also improve thermal shock, which is very much required in sub-entry nozzles (Ye et al., 2004). It also gets oxidized at temperatures higher than 1400°C, therefore its addition was kept to only 1 wt% in all castable matrixes. In the current work, X-ray diffraction results confirmed several crystalline calcium-aluminate phases. Physico-mechanical properties, such as apparent porosity (AP), bulk density (BD), hot modulus of rupture (HMOR), cold modulus of rupture (CMOR) and cold crushing strength (CCS) of hydrated as well as sintered castables of prepared castables, were studied. The sintered castables were also characterized for their microstructure using SEM (scanning electron microscopy).

6.2 Experimental procedure

6.2.1 Material characterization

The starting raw materials were aluminum oxide, calcium carbonate, zirconium dioxide of A.R. grade, procured from Loba Chemie Pvt. Ltd., Mumbai India. The materials were used as received. Commercially available high alumina cements (CA-25 C and CA-14 M), provided by Almatis, Kolkata were also used for comparative study. The Chinese bauxite, reactive alumina and silicon carbide powders were supplied by Shiva Minerals Pvt. Ltd., Rajgangpur, India. The calcined bauxite contained minimum 88.60%, 4.78%, 1.58%, 4.0%, 0.26%, 0.08% and 0.70% by weight of Al_2O_3, SiO_2, Fe_2O_3, TiO_2, CaO, Na_2O and others, respectively.

6.2.2 HAC powder preparation and phase analysis

Commercially available Al_2O_3 and $CaCO_3$ powders were used as the starting materials to prepare the initial mixes in the ratio of 7:3 and 8:2 wt. % of Al_2O_3 and CaO, respectively. The milling operation was carried out in a QM-1SP4 type planetary ball milling system in air at room temperature for 1h, 2h and 3h respectively. A total number of 80 stainless steel balls with a diameter of 10 mm and 2 stainless steel balls with a diameter of 20 mm were used as a milling medium in a 500 ml stainless steel vial. The milling speed was set at 600 rpm. All of the samples were prepared in a glove box before the milling procedure to avoid moisture absorption. The mechanochemically prepared powders were isothermally heat treated (calcined) at the rate of 5°C/min in air atmosphere with 1h holding time at 1000°C. Figure 6.1 shows the flow chart of HAC powder preparation.

The phase composition and crystal structures of the prepared powders were investigated at room temperature using X-ray powder diffraction measurements. X-ray powder diffraction data were recorded at ambient conditions on a high resolution laboratory X-ray powder diffractometer at 40 kV and 40 ma. All the X-ray samples were contained in low absorbing glass capillaries of 0.3 mm diameter and

sealed in a glove box under argon atmosphere using a hot wire. Data were taken in steps of 0.008 2θ from 15 to 50 2θ at 1˚/ min. The samples were spun during measurement for better particle statistics. A qualitative phase analysis using the PDF-2 database (ICDD, 2003) was used to identify the phases. Crystallite size, d of calcined powder was calculated from X-ray line broadening analysis using the Scherer's formula:

$$d = \frac{0.9\lambda}{\beta \mathrm{Cos}\theta}$$

where, β is the full width at half maximum (FWHM) intensity of a Bragg reflection excluding instrumental broadening, λ is the wavelength of the X-ray radiation and θ is the Bragg angle. β is taken for the strongest Bragg's peak corresponding to 2θ. A qualitative phase analysis using the PDF-2 database (ICDD, 2003) was used to identify the phases. The microstructural analysis was carried out using scanning electron microscope (SEM). Bright field transmission electron microscope (FEI, Eindhoven, Netherlands) equipped with SIS Mega View III CCD camera at 120 KV employing analysis software (SIS, Muenster, Germany) was used for TEM investigations. Powder samples for TEM were first dispersed in suitable solvent by ultra-sonication and then dropped on a conventional carbon coated copper grid.

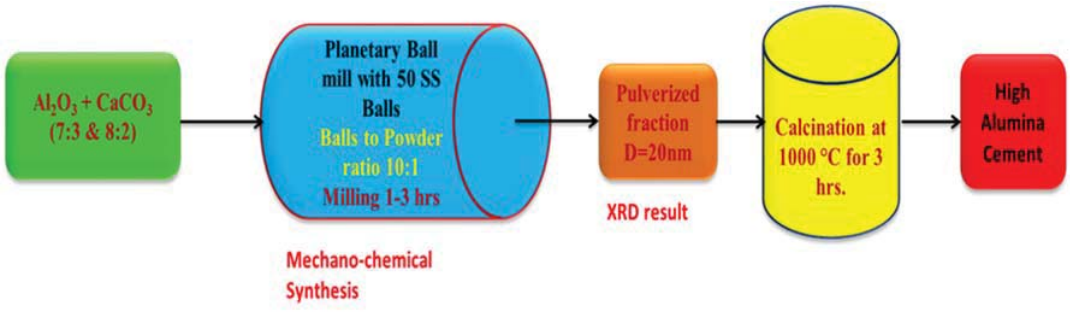

Figure 6.1: Flow chart of HAC powder preparation.

6.2.3 Setting time test

Calcined powders were tested for Initial and final setting by Vicat's equipment according to ASTM C-403. Both the initial and final setting time of high alumina cement were examined by Vicat's apparatus.

6.2.4 Castable formulation

Low cement refractory castables were prepared using 5 wt% prepared HAC cements, 7 wt% water and rest as refractory bauxite. Small additions of zirconia, reactive alumina and micro-fine silicon carbide powder particles were done as pore filling agents. The formulation is summarized in Tables 6.1 and 6.2, showing the detailed compositions with their names. Bauxite particle size distribution is shown in the figure 6.2. In the first step for cement castable formulation, calcined bauxite was oven dried, crushed and grounded in a planetary ball mill for grading into different sizes. The particle size distribution has an important role in the properties of refractory castable. Incorrect particle size distribution may cause militancy or the excess water required by the castables. The particle size distribution of the fine fraction is generally a representation of the flow characteristics. The use of particle packing principles provides the basis of the development of castable with low porosity, means for achieving high compaction in castable. The fine materials replace the part of cement of conventional castables. These micro-fine materials play three major roles; first to fill up the voids between cement particles which reduce the water requirement for achieving the same consistency and also reduces the porosity thereby, increasing density. Secondly, these fine particles have shown some effect on fluidity. Thirdly, the nature of fine particles has shown some effect on the phase composition of the matrix at elevated temperature. Thus, the nature of ultra-fine particles decide the high temperature properties, like creep behavior, corrosion resistance and hot strength.

The trials of aggregate proportions were taken in a 1000 cm^3 flask filled up to 250 cm^3 and vibrated for 45 sec and the packing density calculations were carried out

for each trial. Aggregates having higher packing densities were chosen for further experiments. In the next step, batches were prepared by taking different grades of materials and additives in the proper proportion and which are summarized in Tables 6.1 and 6.2. The materials were dry mixed in a plastic container for 20 min and then were taken for sample preparation. The casting was done by adding the first two-thirds proportion of water at a time. Then, remaining of water was added slowly to get a homogeneous mixing. The wet mixing was performed for up to 8-10 min to achieve proper flow. Immediately after wet mixing, the castable mix was filled into a rectangular bar shape mold (152×25×25 mm) made of hard steel. The mold was placed on the vibrating table filled with the wet mixed castable. It was vibrated for 20 min resulting in better compactness. Several samples of each composition were prepared for laboratory test.

Figure 6.3 shows the flow chart of whole process of low cement castable preparation. The samples were cured in a humidity chamber (95% RH) at room temperature for different time periods. Before firing the samples, they were first oven dried at 120°C for 24 h. The test samples were fired at 1300-1550°C with a variation of ±5°C in an electric SiC heating element furnace with a soaking time of 3h. The cured samples as well as the fired samples were tested for BD, AP, TSR, HMOR, CMOR and CCS. These samples were also analyzed by XRD for crystalline phases present and by SEM for their morphological behavior. The commercialized cement castables were also prepared for comparison purposes.

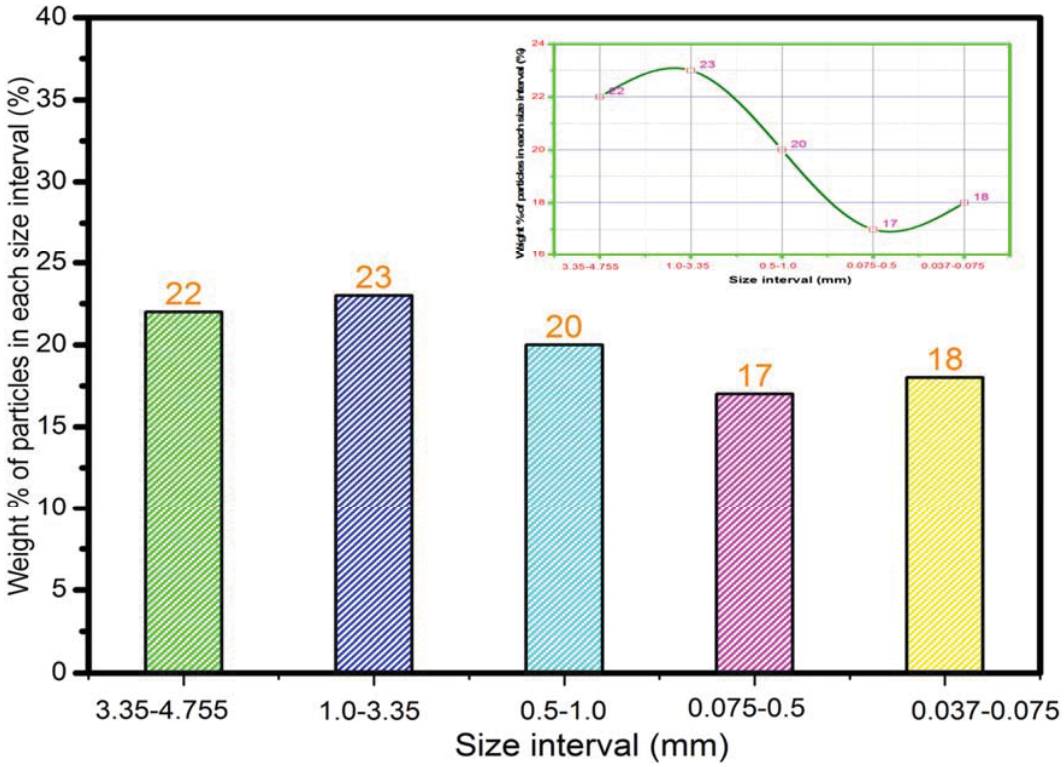

Figure 6.2: Bauxite particle size distribution.

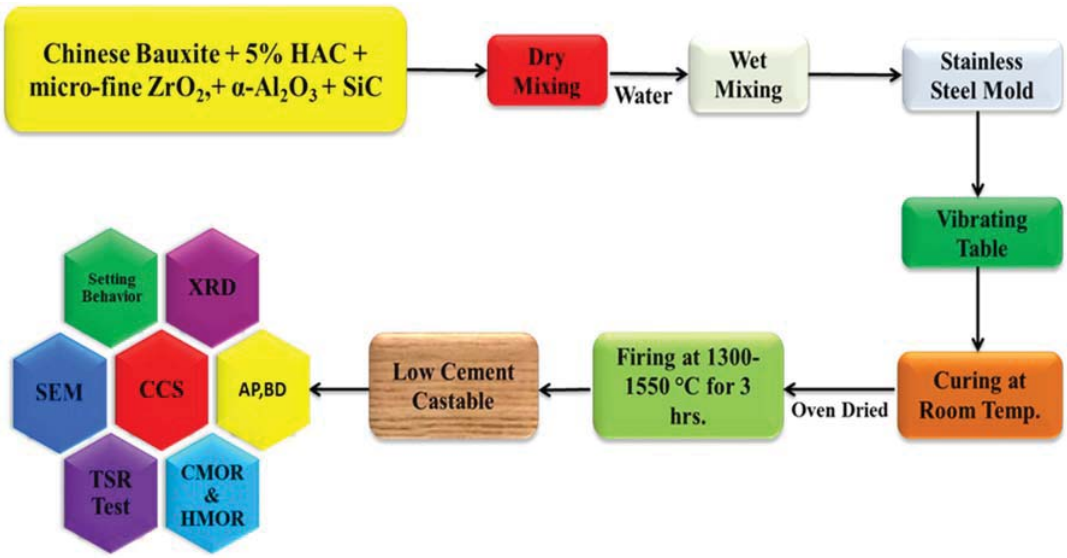

Figure 6.3: Flow chart of low cement castable preparation.

Table 6.1: Batch composition with HAC70.

Sample	HAC70 (Wt %)	Chinese Bauxite (Wt %)	α-Al_2O_3 (Wt%)	Microfine ZrO_2(Wt %)	Microfine SiC (Wt %)
P1	5	80	14	0	1
P2	5	80	12	2	1
P3	5	80	10	4	1
P4	5	80	8	6	1
P5	5	80	6	8	1
P6	5	80	4	10	1
P7	5	80	2	12	1
P8	5	80	0	14	1

Table 6.2: Batch composition with HAC80.

Sample	HAC80 (Wt %)	Chinese Bauxite (Wt %)	α-Al_2O_3 (Wt%)	Microfine ZrO_2 (Wt %)	Microfine SiC (Wt %)
Q1	5	80	14	0	1
Q2	5	80	12	2	1
Q3	5	80	10	4	1
Q4	5	80	8	6	1
Q5	5	80	6	8	1
Q6	5	80	4	10	1
Q7	5	80	2	12	1
Q8	5	80	0	14	1

6.2.5 Cold crushing strength of HAC and LCC formulated

CCS of cement was measured as the compressive strength of a 50 mm cement cube made of pure HAC (without any aggregates).These samples were tested for compressive strength after 6 h, 24 h and 7days, respectively, according to (ASTM C1194-03).

6.2.6 Cold and hot modulus of rupture (CMOR and HMOR) of LCC formulated

Cold and hot modulus of rupture measurements were carried out under three-point bending tests(ASTM C133-97for CMOR and ASTM C583-10for HMOR)using dimension 152mm × 25mm × 25mm of samples. CMOR and HMOR were calculated using the following formula:

$$\mathrm{MOR} = \frac{3\mathrm{PL}}{2\mathrm{db}^2}$$

CMOR tests were carried out at room temperature using UTM machine (Model 810, MTS System, Eden Prairie, MN, USA)for samples pre-fired at 1300˚C, 1350˚C, 1400˚C, 1450˚C, 1500˚C and 1550˚C for 3h.HMOR measurements were made at 1400˚C, 1500˚C and 1600˚Cusing Netzsch414/3 HMOR Equipment (Netzsch Selb, Germany) for samples pre-fired at 1550˚C for 3 h, cooled at room temperature and then reheated for testing.

6.2.7 Bulk density, apparent porosity, thermal shock cycles and SEM of prepared castables

Apparent porosity and bulk density were determined according to ASTM C20-00 which involves boiling water bath principle. Cyclic thermal stability of the refractories was determined experimentally by water quench test; ASTM C1171-05.The thermal shock resistance (TSR) is measured by the number of cycles a specimen survives without any visible damage appearance, when the specimens are subjected to thermal cycling. This effect was evaluated after each cycle of consecutive firings at 1000°C and then subsequent water quenching at 25°C for 20

min. This firing was done in an electric furnace containing SiC heating elements. The microstructural evolution of castables fired at 1550°C was examined using field emission scanning electron microscopy of representative regions of fractured specimens. All samples were prepared after initial grinding, further grinding was done in two steps, i.e., with 240, 320, 400 and finally 600 grit SiC abrasive paper. The samples were then polished on velvet cloth impregnated with 6 microns and finally with 1 micron diamond paste. Water was used as a lubricant. After final polishing samples were etched with mixture of HCl and HNO_3. These samples were then coated with carbon unit to make them conductive. Silver paste was used on the corners of the samples to avoid any charging during testing.

6.3 Results and discussion

6.3.1 Evolution of phases by X-Ray diffraction

Figure 6.4 shows the XRD patterns of a mixture of Al_2O_3 and $CaCO_3$ milled for different time durations. For the samples milled for 1 h to 3h, the diffraction peaks visible are attributed to $CaCO_3$. These significant peaks even after 3h of intense milling in the planetary mill can be taken as a further indication of the high milling resistance and mechanical strength of their nano particles. No Al_2O_3 peak is evident as it exists in amorphous phase. $CaAl_2O_4$ diffraction peak is also not observed indicating no phase formation at this stage. Nano-meter range powder is formed as a result of high energy ball milling when attrition time increases to 3 h. Figures 6.5 and 6.6 demonstrate the XRD patterns of samples calcined at 1000°C with 70 and 80 wt. % alumina termed as HAC70 and HAC80, respectively. Pure crystalline cementing phases only begin to form when the temperature is 1000°C in both HAC70 and HAC80 compositions. A major improvement in crystalline behavior is evident when both cement samples were fired at 1000°C. Prime phases investigated in both compositions include CA, CA_2 and CA_6, which are readily formed and thermodynamically most stable compounds in the CaO-Al_2O_3 binary system. These peaks were identified by standard JCPDS cards numbered 88-2477, 89-3851 and 07-0085 for their corresponding peaks of monoclinic CA, CA_2 and hexagonal CA_6, respectively. In the conventional preparation route by high-temperature solid-state synthesis, the batch usually contains CaO-rich phases and un-reacted Al_2O_3 before the appearance of desired product phase. The formation sequence of phases in these mixtures is always from calcia-rich phases to the alumina rich phase. Presence of broad peaks in XRD patterns of calcined cement powders shows that the particle size is small.

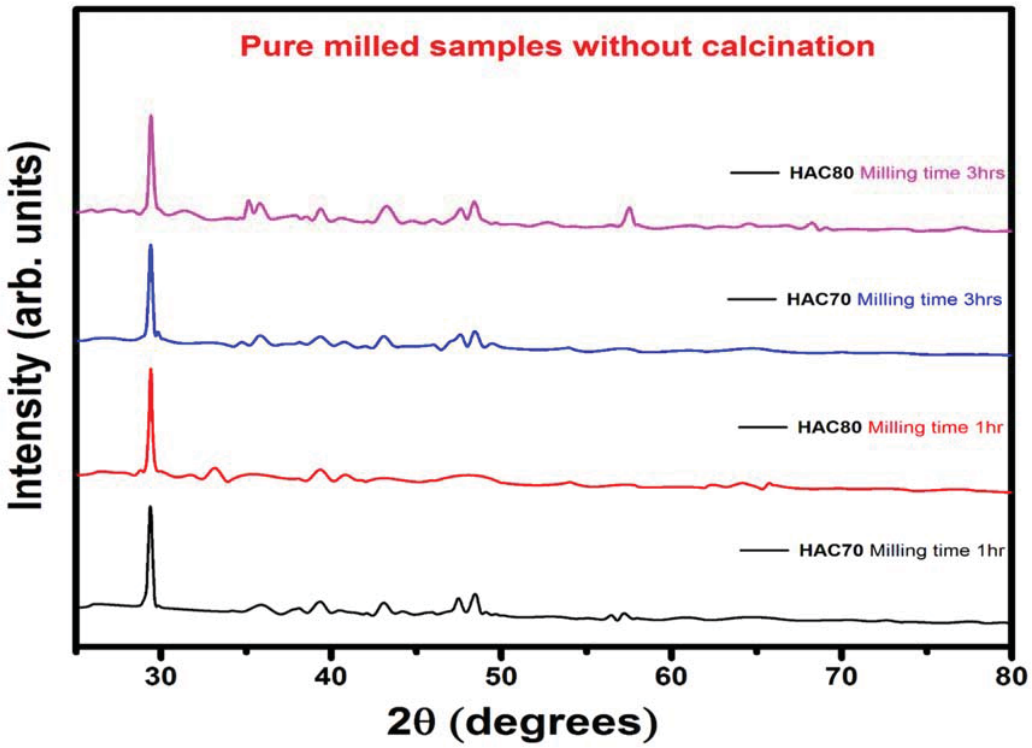

Figure 6.4: XRD plot of pure milled HAC powder.

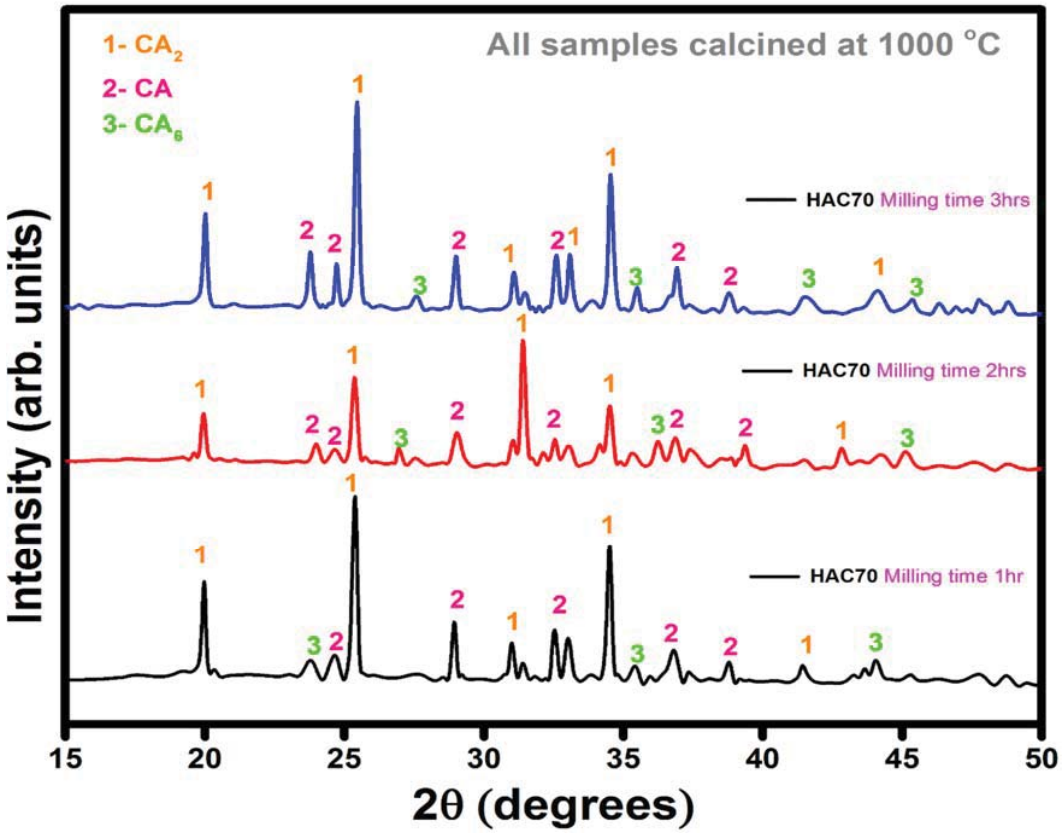

Figure 6.5: XRD plot of HAC70.

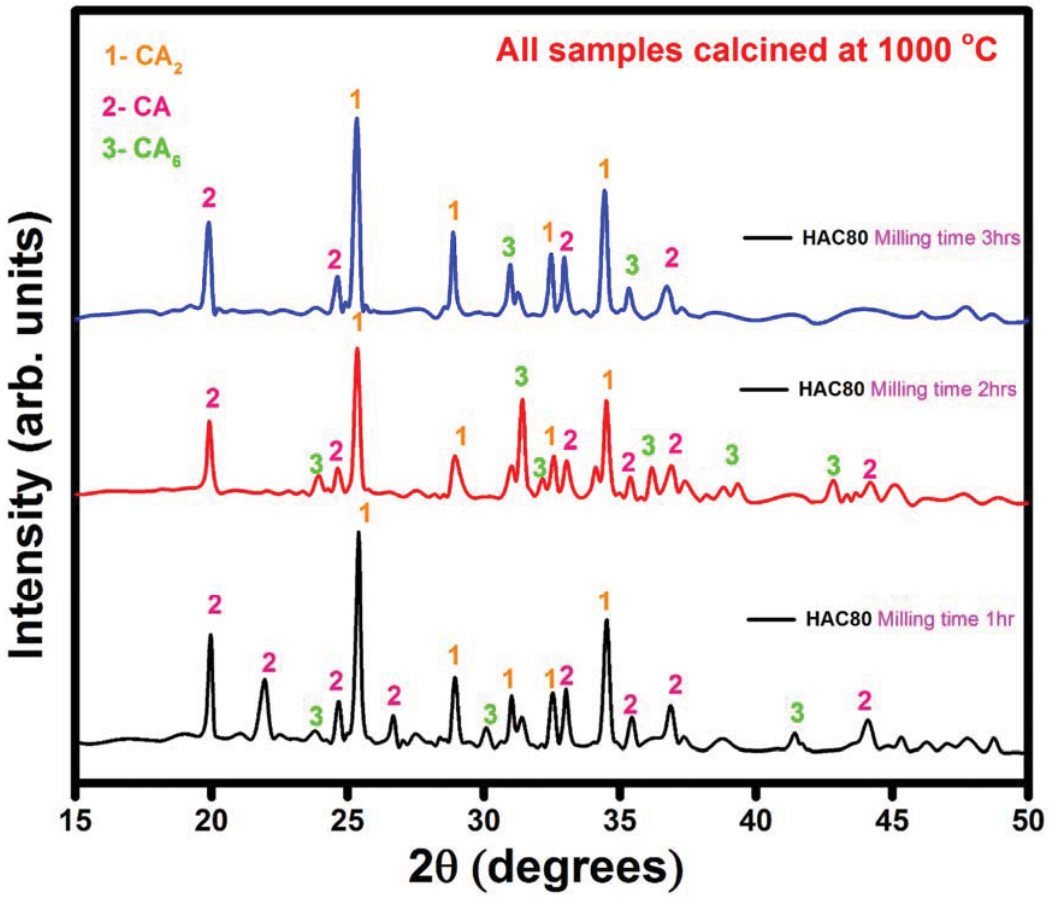

Figure 6.6: XRD plot of HAC80.

6.3.2. Setting behavior of HAC

Figure 6.7 shows the setting behavior of HAC. The prepared HAC powders were mixed with water (0.85 P). At room temperature (26°C), 70 wt. % alumina containing cement gave an initial setting time of 28 min and final setting occurred in 57 min. Second composition of HAC having 80 wt. % alumina had an initial setting time of 36 min and a final setting time of 78 min. In initial curing stage, the strength is obtained by coagulation of the polyvalent ion from the alumina cement. This initial set provides sufficient strength for the core (frame mold) removal. It is observed that with increasing alumina content the setting time exhibited an increasing trend. High alumina content results in increased formation of CA_6, which

does not take part in hydration reaction but is necessary for high temperature strengths. Presence of this phase increased the setting time of the prepared cement in comparison to standard commercial products and thus an improvement in workability of cement pastes was observed.

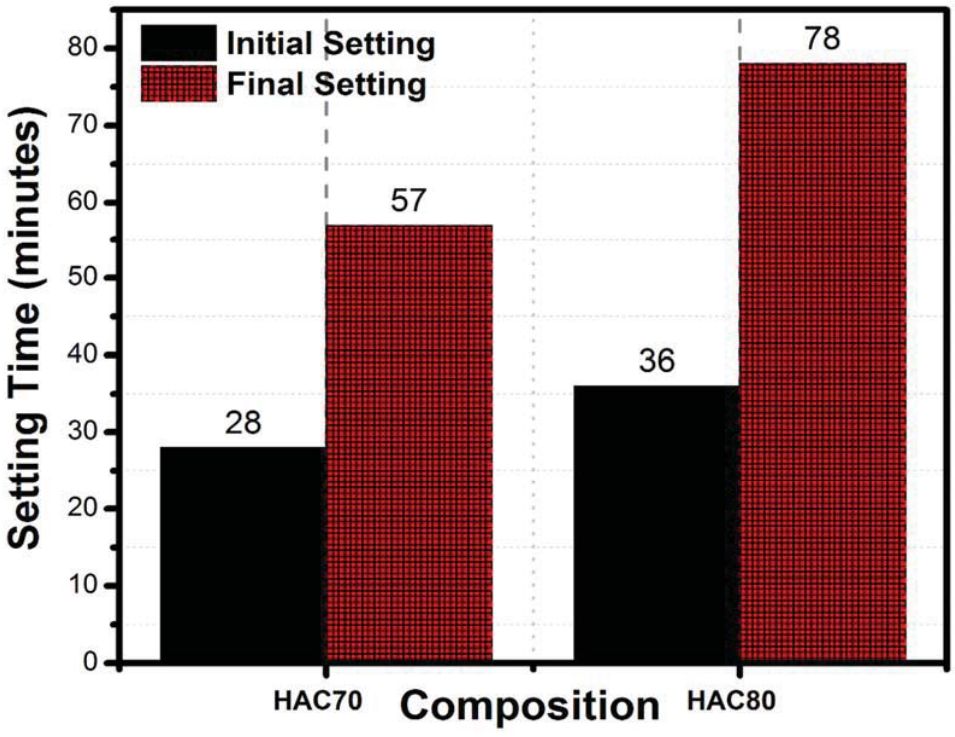

Figure 6.7: Setting time behavior of HAC70 and HAC80.

6.3.3 CCS of HAC fired at 1000˚C

The pure high alumina cement attained good structural strength as presented in figure 6.8. Samples were tested after curing for 6 h, 24 h and 7 days. Sample blocks of two commercialized cements of similar compositions were also prepared to have a better comparative result. The strength increased rapidly with curing time in all the compositions. Initially, in 6 h, the CCS value obtained for HAC70 is 12 MPa and for HAC80 is 15 MPa. After7 days it reached up to 89 and 96 MPa for HAC70 and HAC80, respectively, which is better than the commercially available CA-14M (76

MPa) and CA-25C (84 MPa). It gets the maximum strength at around 7 days and after this period there is a very slight variation. It can be seen that HAC80 samples have more compressive strength than the HAC70 sample. The higher strength of HAC80 is ascribed to the presence of larger amounts of CA_6. It is a well-known fact that mono-calcium hexaluminate (CA_6) phase is very stable and high temperature sustaining phase. The most significant advantage of this phase is its needle and platelet like morphology growth, which is rarely formed through novel low temperature diffusion mechanism. Improved mechanical properties result from in situ whiskers or platelets formation. Dispersion of shaped CA_6 within the matrix enhanced crushing strength by crack defection and grain bridging mechanisms. These mechanisms dissipate considerable strain energy through frictional motion of the reinforcement phase against the matrix during elastic stretching, debonding and pullout (De La Iglesia et al., 2012). Thus, an increase in the number, diameter and debond length of such bridging reinforcements is expected for the enhanced toughening effects (Domoanguez et al., 2001). Although CA_2 is known to react slowly with water in the early stages of hydration, its presence along with other phases results in an overall faster hydration rate as the heat of hydration resulting from the hydration of CA activates CA_2 and makes it react relatively faster with water than it would do alone. Present outcomes are efficacious and analogous with mineralogical studies by XRD, exhibiting high structural strength in both the samples. This is due to the formation of the stable ceramic bond and the absence of any impure phase.

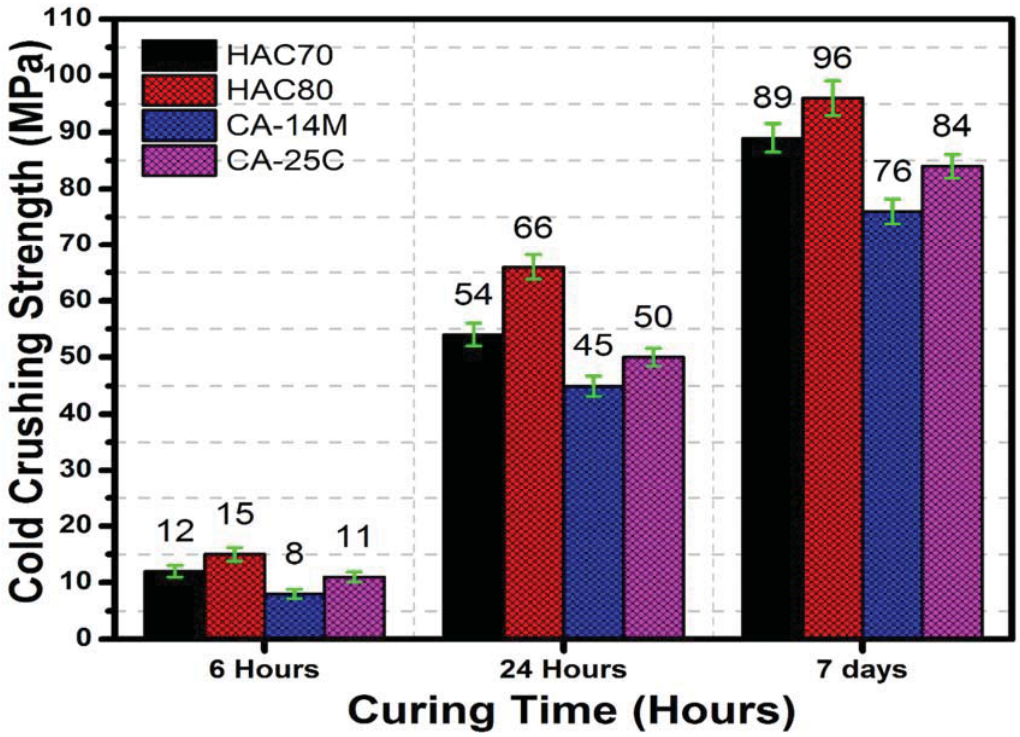

Figure 6.8: Cold crushing strength of HAC70 and HAC80.

6.3.4 SEM of HAC

Figures 6.9 and 6.10 represent the SEM of networks of well-crystallized interlocking hexagonal plates of CA matrix of HAC70 and HAC80 fired at 1000°C, respectively. In both figures, a, b, c and d represent different magnifications of the same samples. The monoclinic phases of CA, CA_2 and hexagonal phase of CA_6 can be observed in both micrographs. High amounts of CA and CA_2 is proposed to enhance the refractory properties. The morphology of CA_6 grains shows preferential growth along their basal plane. After CA_6 formation, the main mechanism responsible for grain growth is the welding of neighboring platelet grains when they are disposed with their flat boundaries, and thus with their basal planes, parallel. For this reason, platelet grains become more equiaxed as firing temperature increases. When grains are equiaxed, the proportion of grains with basal planes parallel is very low, so the increase in firing temperature does not much affect grain granulometry. Figures 6.9

and 6.10 illustrate the presence of both mechanisms; grain impingement and plate welding. CA_6 phase is responsible for high strength at high temperature without rapid physical and chemical deterioration. Major parts of trigonal crystals in cementing phase are evident in the most homogeneous distribution of CA and CA_2 phase matrix.

Figure 6.11 shows the particle size and crystallinity of the prepared HAC80 powder produced by mechanochemical synthesis which was investigated by TEM. Numerous crystals were isolated in dispersed form, mostly in perfect spherical shape. Their growth along their circumference indicates that reaction propagated equally from all directions providing sufficient room for overall circumferential growth. HAC80 produced the loosely agglomerated fine particles of an average 40 nm diameter.

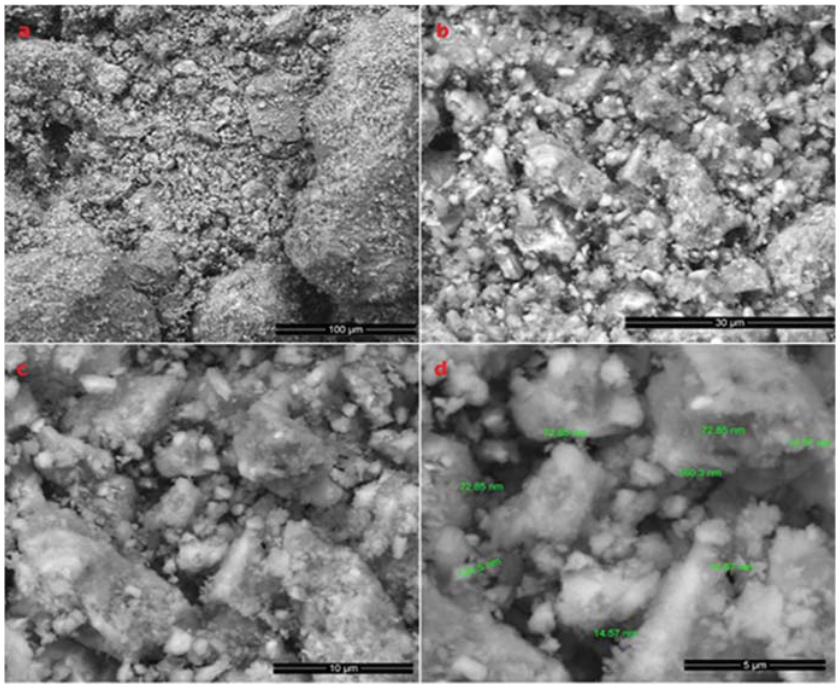

Figure 6.9: SEM of HAC70.

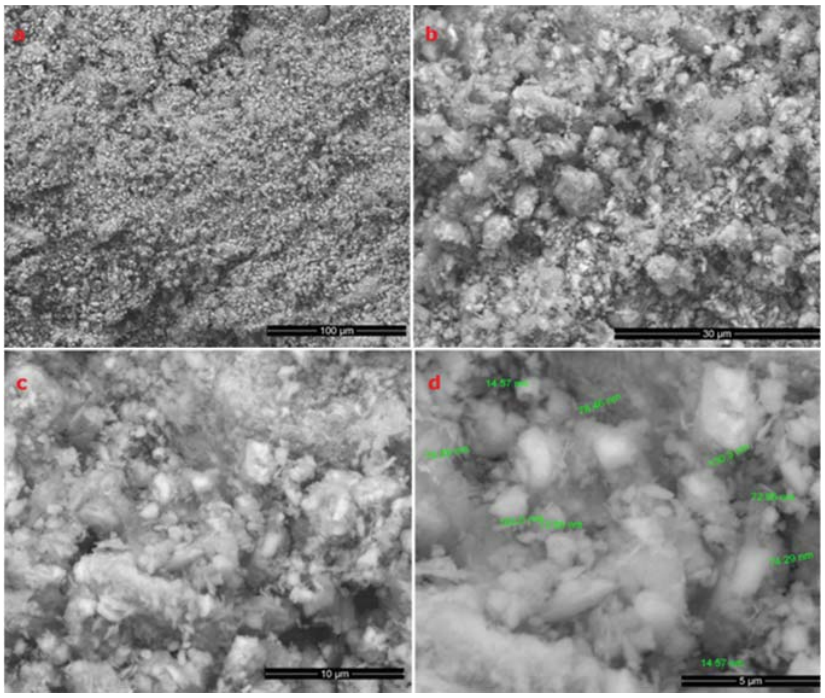

Figure 6.10: SEM of HAC80.

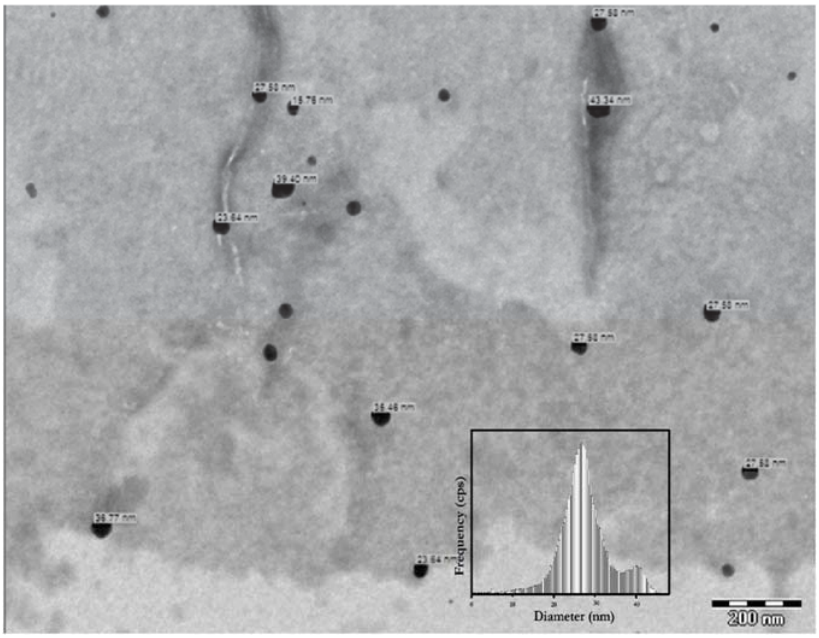

Figure 6.11: TEM of HAC80.

6.3.5 XRD patterns of castables fired at 1550˚C for 3h

X-ray diffraction patterns of sintered samples of prepared high alumina cements based castables were observed to estimate the phases present after sintering at 1550°C temperature with same soaking period. End point of reactions, occurring during sintering, was estimated from the amount of the different phases present. X-ray diffraction was done for all samples and the results were correlated with the reaction behavior and phases formation. Figures 6.12 and 6.13 portray X-ray patterns of castables fired at 1550°C for 3 h. Here P (1-8) and Q (1-8) indicate the series of castables formulated with HAC70 and HAC80, respectively. The corundum phase appeared as a major component due to the transformation of bauxite minerals to corundum. Other major phases detected were zirconia and mullite. Silicon carbide also occurred as a minor peak, which was in correlation with the slight addition of silicon carbide in all the castable samples. In both castable series P and Q, as we proceed from high to low batch number, the peak intensities increase; this is accounted for increasing micro fines. These peaks were identified by standard

JCPDS cards numbered 46-1212 (Al_2O_3), 15-0776 ($3Al2O_3.2SiO_2$), 42-1091(SiC) and 78-1807 (ZrO_2).

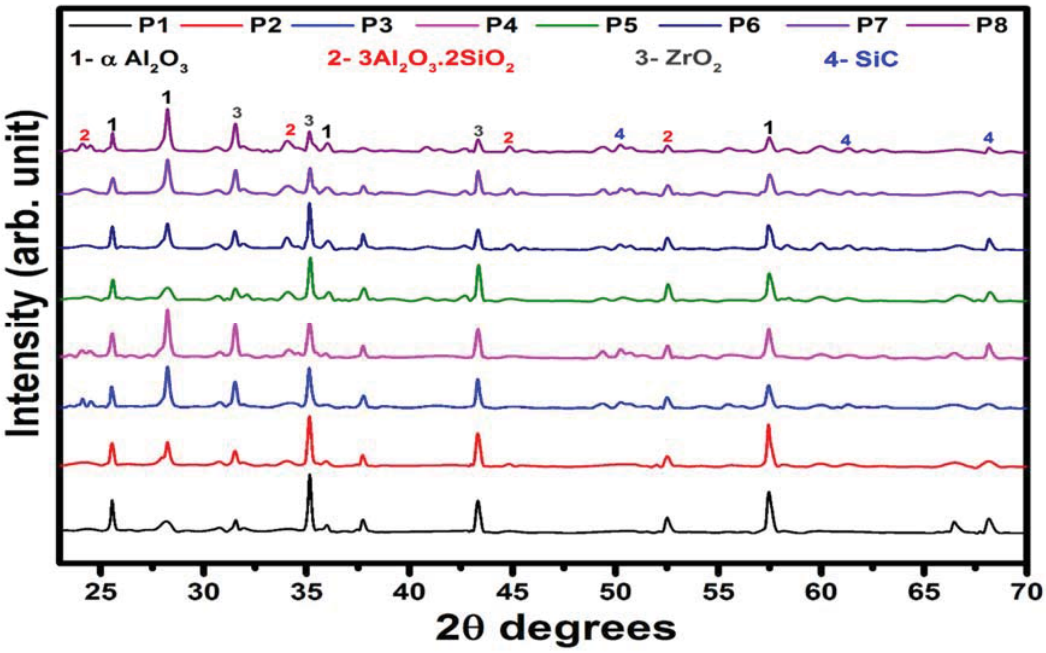

Figure 6.12: XRD plot of P series castables prepared with HAC70.

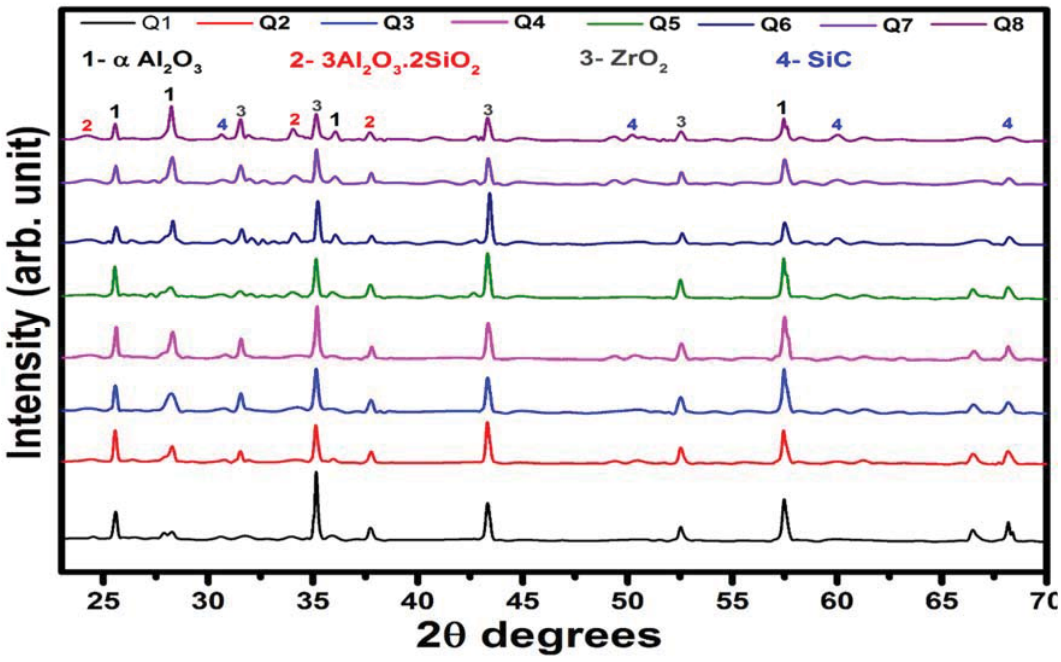

Figure 6.13: XRD plot of Q series castables prepared with HAC80.

6.3.6 Bulk density, apparent porosity and thermal shock cycles of prepared castables

Table6.3 displays the values corresponding to bulk density, apparent porosity and thermal shock of P6 and Q6 series castables sintered at varying temperature range. Only these series were selected as homologous to their other thermo-mechanical superiority. In the castables prepared, highest bulk densities achieved are 3.31g/cm^3 and 3.42 g/cm^3 for the compositions P6 and Q6, respectively as when compared with 3.21g/cm^3 and 3.32 g/cm^3 of their commercial cement based castable counterparts. This can be attributed to the use of higher percentages of micro-fine ZrO_2, α-Al_2O_3 and SiC in the aggregate as well as CA_6 formation. Apparent porosity was measured to be in the range of 6.6%–9.6% in the castables prepared, though it was 9.1 and 7.8 for P6 (CA-14 M) and Q6 (CA-25C), respectively. Table6.3 shows the number of thermal shock cycle values evaluated for P6 and Q6 series castables. This series was chosen in agreement with their superior mechanical

properties. All the Q and P series samples exhibited high spalling resistance completing 10 cycles while P6 and Q6 attained 19 and 22 cycles, respectively. Commercial cement containing castables also achieved 18 cycles.

Table 6.3: Bulk density, apparent porosity and thermal shock cycles of prepared castables.

Test Method	Temperature (°C)						
	Sample Name	1300	1350	1400	1450	1500	1550
Bulk Density (gm/cc)	P6	2.90	2.95	3.00	3.25	3.28	3.31
	P6(CA-14 M)	2.85	2.91	2.96	3.21	3.15	3.20
	Q6	3.05	3.15	3.26	3.35	3.39	3.42
	Q6(CA-25C)	2.94	3.05	3.16	3.26	3.30	3.32
Apparent Porosity (%)	P6	9.6	9.5	8.8	8.6	8.2	8.0
	P6(CA-14 M)	11	10.6	9.8	9.4	9.2	9.1
	Q6	7.9	7.8	7.6	7.5	7.1	6.6
	Q6(CA-25C)	9.2	8.8	8.5	8.2	8.1	7.8
Thermal Shock Cycle	P6	18	15	15	14	15	19
	P6(CA-14 M)	17	16	14	12	14	18
	Q6	19	17	16	15	16	22
	Q6(CA-25C)	16	15	17	12	14	18

6.3.7 CCS of different castable compositions sintered at 1300˚C –1550˚C for 3 h.

Prepared high alumina cement was used for formulating low cement castables according to the Tables 6.1 and 6.2. Micro-fine ZrO_2, α-Al_2O_3 and SiC content has been varied, which according to plots resulted in corundum and mullite phase formation along with existing phases. This formation of phases also has a varying effect in the CCS of the castables formulated. Figure6.14 depicts the castable series Q and P. High values of CCS ranging 160-282MPa was achieved at the maximum sintering temperature 1550°C for Q series castables. Similarly, 156-279 MPa was achieved for P series castables. Figure 6.15 represent a comparative crushing strength plot of Q6 and P6 castables prepared with synthesized and commercial cement. It can be predicted that the rise in sintering temperature has a positive effect on the mechanical properties of both series of castables. Formation of

corundum as well as the addition of zirconia strengthens the structure at high temperatures and the mullite solid solution helps in increasing structural strength. Silicon carbide also plays very important role in improving the CCS value of all the castable. The CCS of the castables prepared with HAC70 and HAC80 were higher in comparison with the CCS of conventional bauxite containing LCC prepared withCA-14 M (136 MPa) and CA-25 C (220 MPa), respectively.

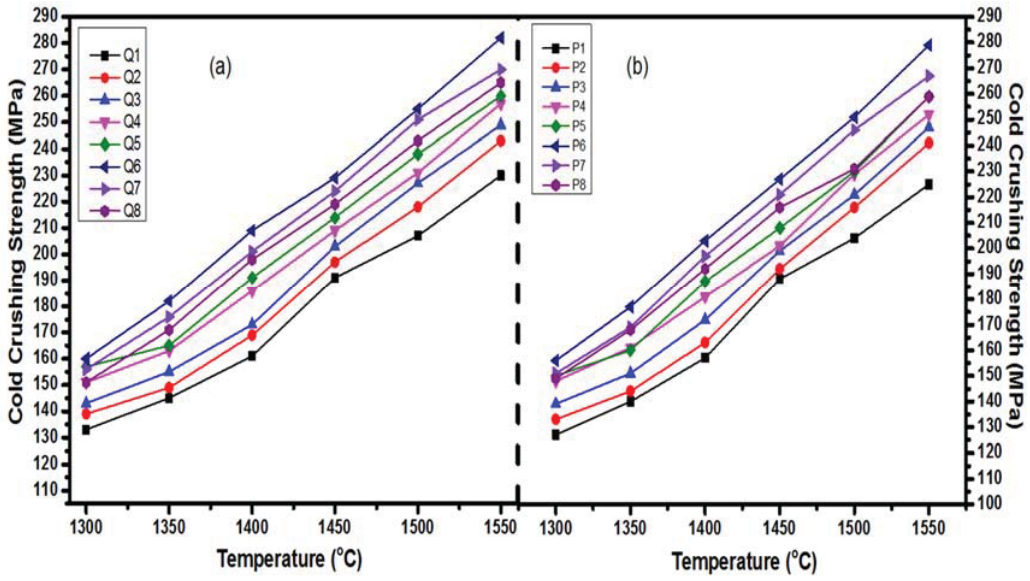

Figure 6.14: (a) Cold crushing strength of Q series of castables; (b) Cold crushing strength of P series of castables.

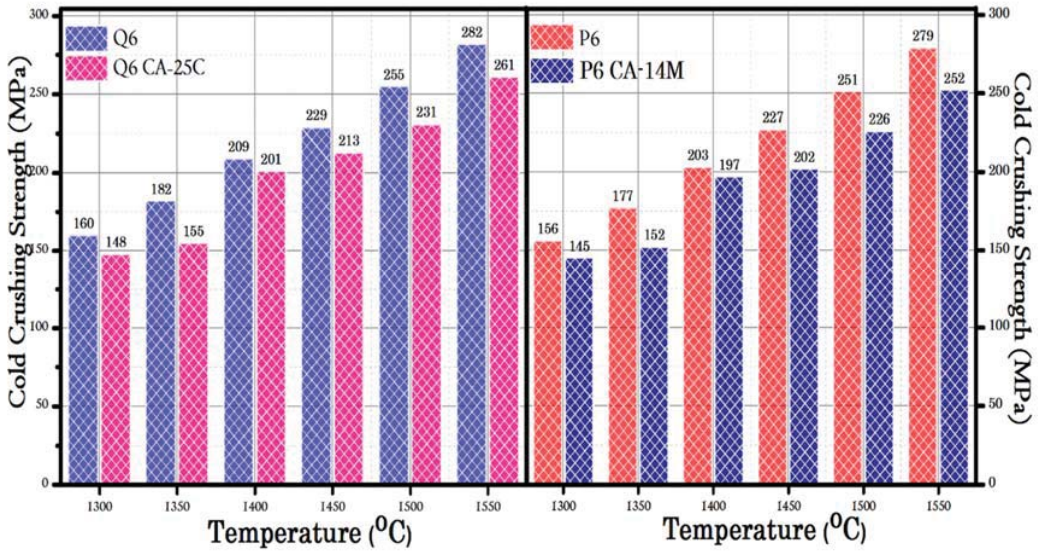

Figure 6.15: Compared cold crushing strength of Q6 and P6 castables.

6.3.8 CMOR and HMOR of different castables

Cold modulus of rupture of Q and P series castables is displayed in figure 6.16. It can be observed that values as high as 82 MPa can be obtained, even if apparent porosities are near 9%. The flexural strength of a ceramic material is linked to both its density and pores morphology. Usually, an increase in firing temperature leads to an increase in density and accordingly in flexural strength. This behavior is followed by both series castables and it is found to be highest for Q6 in which maximum amount of corundum, mullite, zirconia and silicon carbide phase was identified. Hot modulus of rupture (HMOR) of castables Q and P series is shown in figures 6.17 and 6.18, respectively. Here, again Q6 achieved the maximum strength at high temperature/load. The increase in HMOR values of few samples from 1400 to 1600°C is due to the increased formation of corundum and mullite solid solutions. To clinch we may say that the safe range for these types of castables at higher loads is lower than 1600°C. The impurities in the bauxite aggregate increase the liquid

phase sintering and decrease the porosity which consequently increases the mechanical properties.

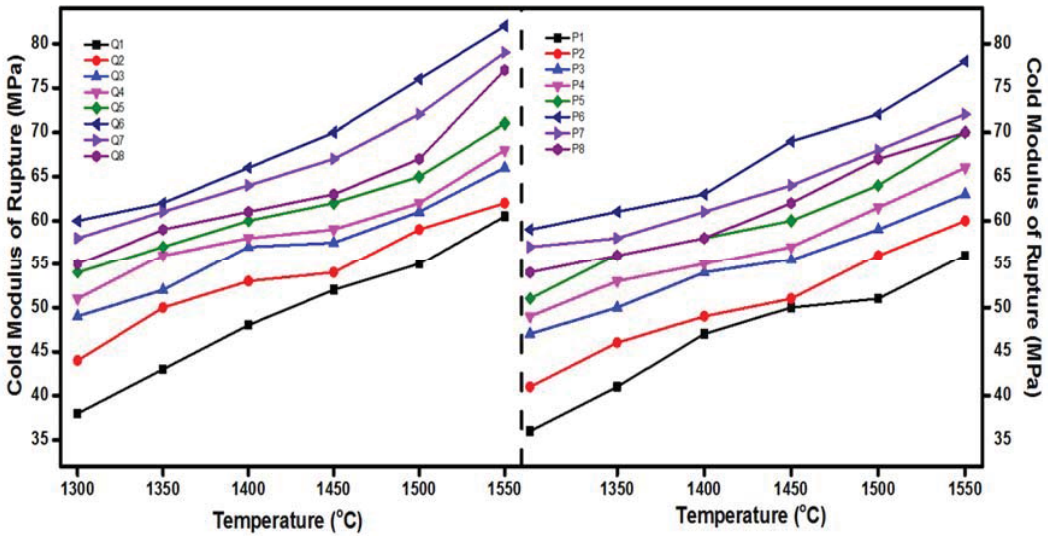

Figure 6.16: Cold modulus of rupture of castables.

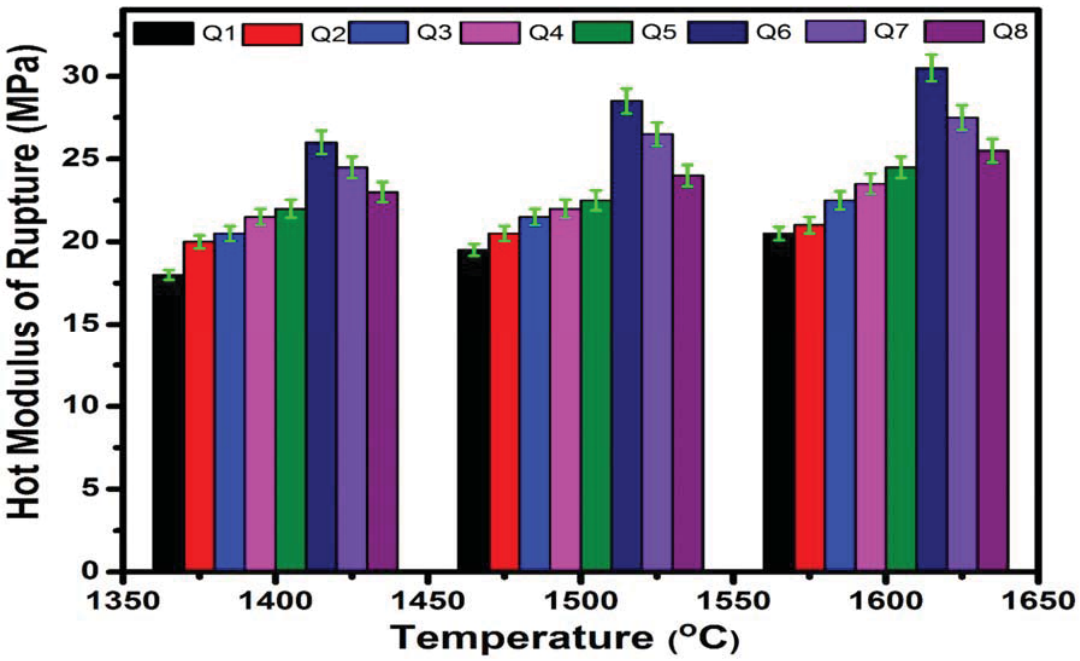

Figure 6.17: Hot modulus of rupture of castables prepared with HAC80.

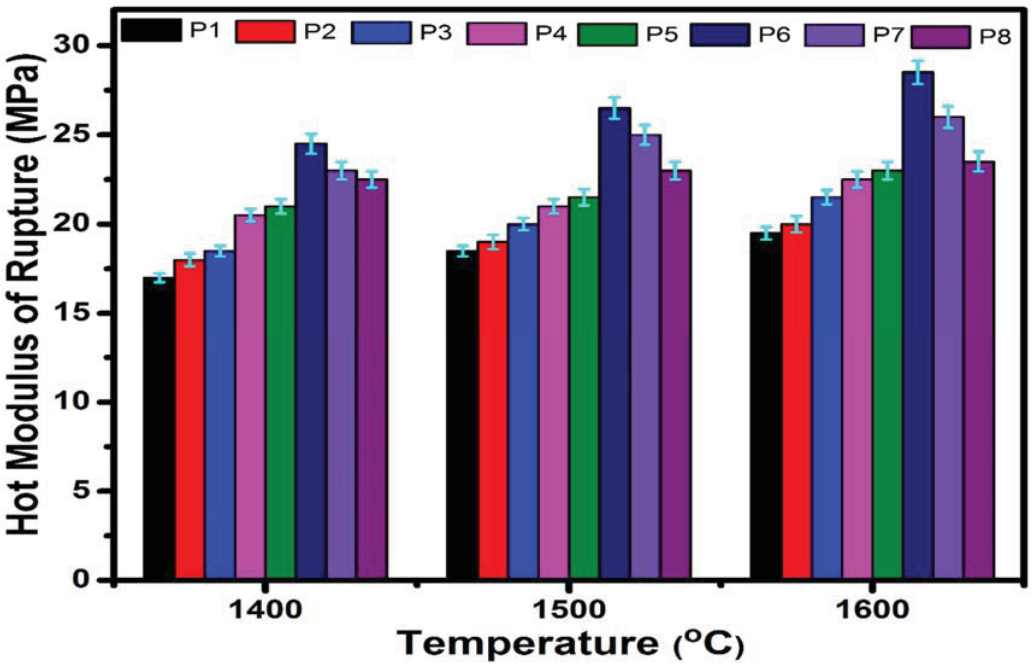

Figure 6.18: Hot modulus of rupture of castables prepared with HAC70.

6.3.9 SEM of Q1-Q8 castable

Figures 6.19 to 6.26 depict the SEM photo micrographs of Q series castables after firing at 1550°C for 3 h, where a, b, c and d represent different magnifications. Only Q series castables were chosen for analysis through SEM as they represented superior thermo-mechanical and physical properties than P series castables. All micro-plots indicate that the examined samples have a dense crystalline structure with a high rate of grain growth of corundum, mullite and zirconia as well as the direct bonding of the same crystals. The presence of abundant corundum trigonal phase is noticed in all microstructures. The high alumina cements bonding phases, which were traced in all 8 compositions, occur in low amounts mainly at the grain boundaries of corundum, mullite and zirconia, so they practically do not reduce the refractoriness of the materials. In figures 6.19 to 6.23, the matrix includes CA and some liquid phases. SEM photomicrographs in figures 6.20 and 6.21 exhibit densely packed microstructure of micronized zirconia, embedded in the trigonal corundum matrix. As we proceed to micrographs figures 6.24 to 6.26, some acicular mullite beside corundum grains appeared in the microstructure. The presence of such in-situ formed phase (mullite) provided interlocking of grains and reinforced the matrix confirming the high strength and refractory properties of castables. The impurities such as silica that was present in Chinese bauxite could be accounted for a mullite solid solution formation, which tend to increase the refractory properties. This property is more evident when we zoom into the microstructures while moving from a to d in each plot. The influence of trace impurities presented during the processing of ceramics is well known and exploited in the control of densification, grain growth and morphology during sintering. The ability to control microstructure is important for achieving the desired properties.

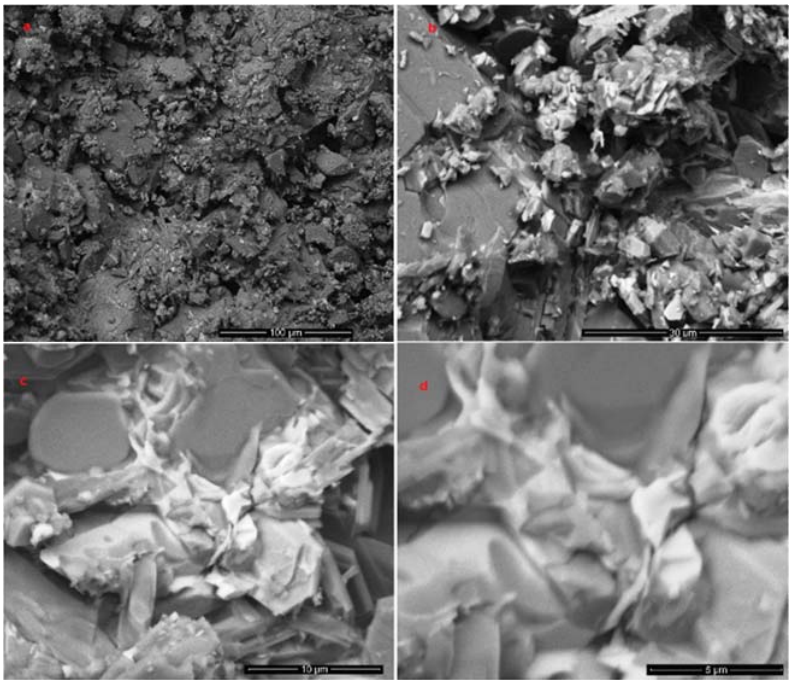

Figure 6.19: SEM of Q1 castable prepared with HAC80.

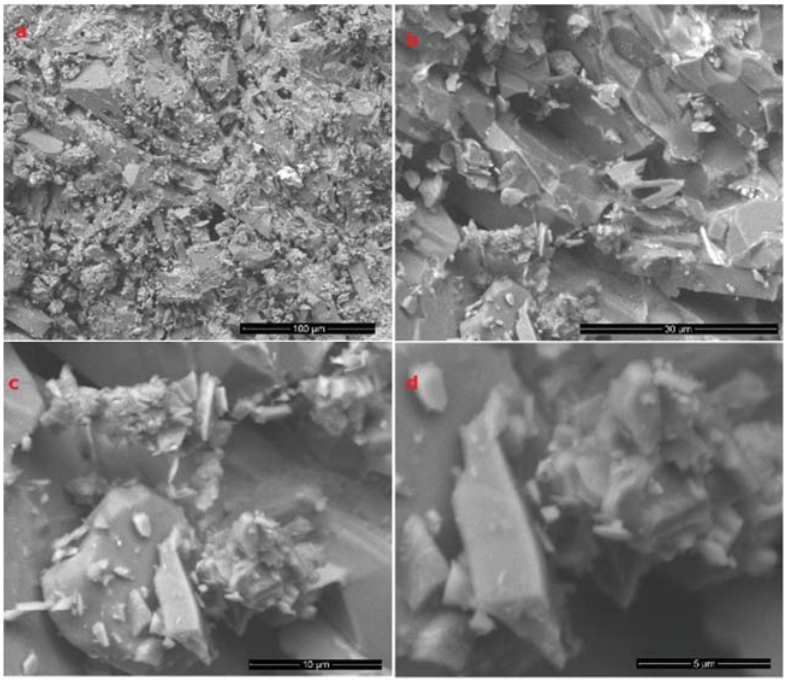

Figure 6.20: SEM of Q2 castable prepared with HAC80.

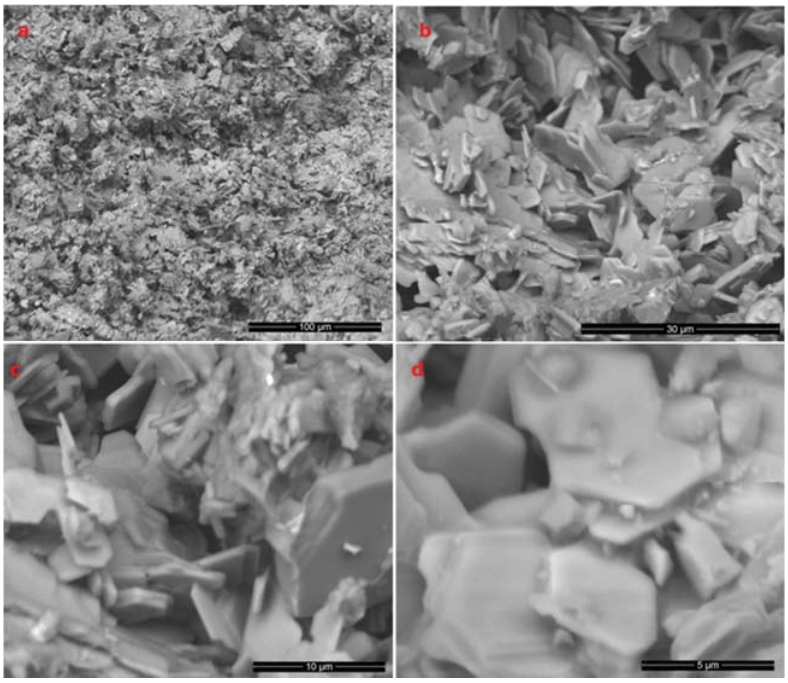

Figure 6.21: SEM of Q3 castable prepared with HAC80.

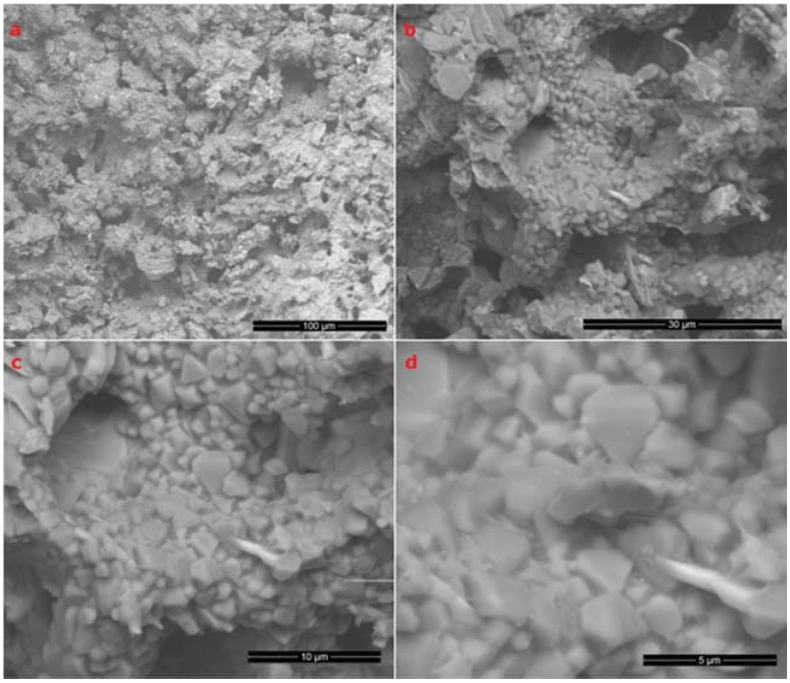

Figure 6.22: SEM of Q4 castable prepared with HAC80.

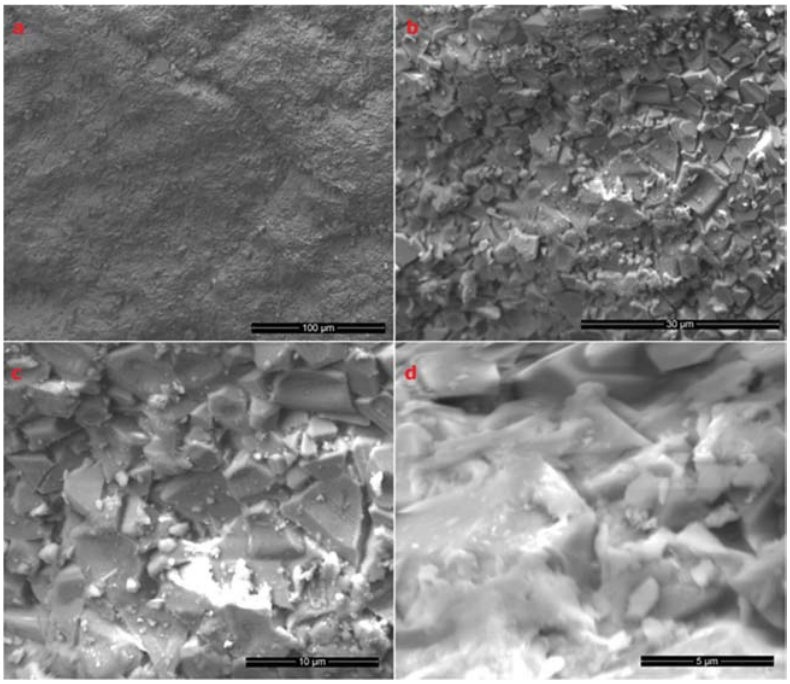

Figure 6.23: SEM of Q5 castable prepared with HAC80.

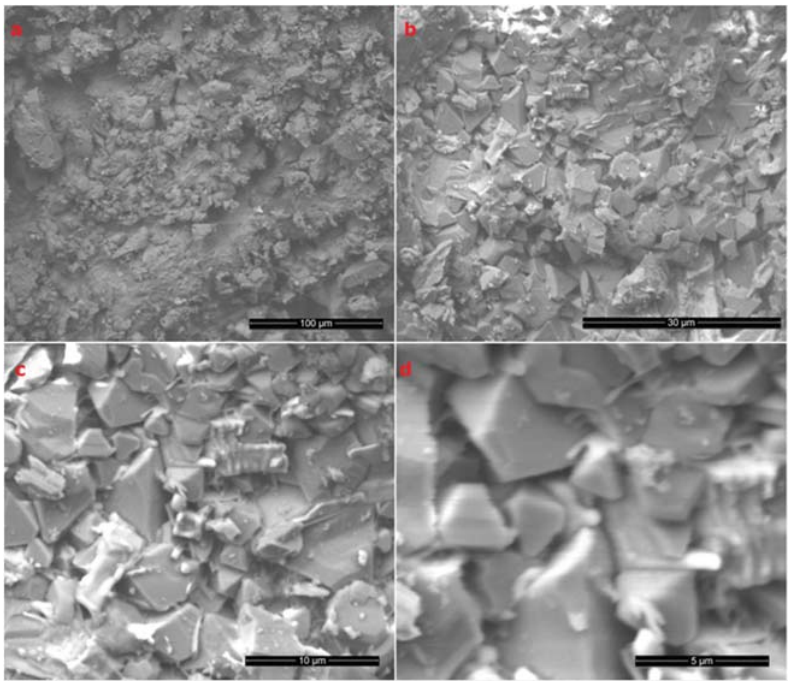

Figure 6.24: SEM of Q6 castable prepared with HAC80.

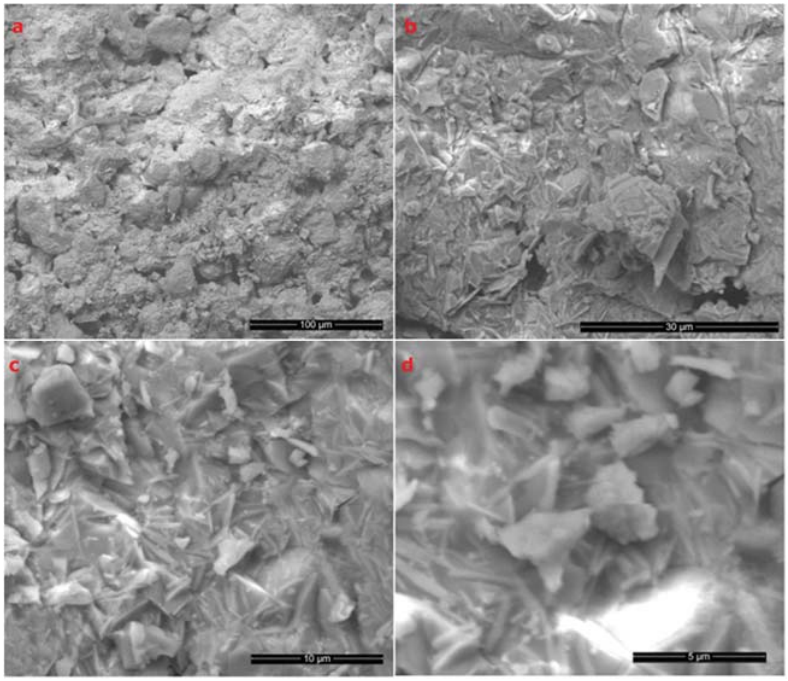

Figure 6.25: SEM of Q7 castable prepared with HAC80.

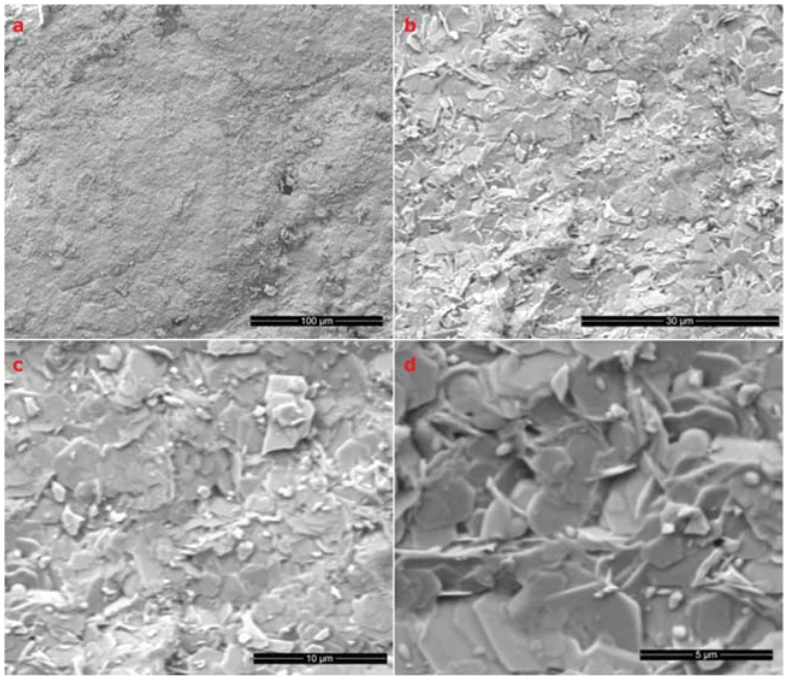

Figure 6.26: SEM of Q8 castable prepared with HAC80.

6.4 Conclusion

In the present section of research work, first high alumina cements were mechanochemically synthesized with subsequent calcination at 1000°C. HACs prepared by this method possessed very small crystallite size. Cementing behavior of these cements promise its commercial implementation. Desired cementing phases, such as CA, CA_2, and CA_6, were formed at lower temperatures. One advantage of this process is to exclude silicate phases, which are the cause behind eutectic formations in such cements. These silicate phases, if any, decrease the refractoriness of the cement and therefore, is not suitable for high temperatures.

The second part of the study was focused on utilization of this prepared cement for formulation of castables. The XRD patterns of castables; containing bauxite, micro-fine ZrO_2, α-Al_2O_3 and SiC showed new and pure phases, such as corundum, mullite along with pre-existing zirconia and SiC. The formation of CA_6 and absence of silicate phases in cement was responsible for superior thermo-mechanical and physical properties when compared with commercial cements containing castables. Castable samples prepared by HAC80 have better mechanical properties than the HAC70 even though it had lower setting time. Trigonal corundum and acicular mullite were formed at high temperatures. These phases facilitated ceramic bonding which resulted in increase of CCS and CMOR values. Regenerated grains of corundum also improved thermal cycles. SEM results showed dense microstructure of all the samples. Some liquid phase is also visualized due to the impurities present in bauxite. These excellent properties of such castables may enable their use in various refractory applications, such as production of steel, aluminum, copper, glass, cement, chemicals and ceramics.